Angewandte Chemie International Edition

Angewandte International Edition Chemie

GDCh German Chemical Society

How to cite: *Angew. Chem. Int. Ed.* **2026**, e23132
doi.org/10.1002/anie.202523132

RESEARCH ARTICLE OPEN ACCESS

Proximity-Induced Transfer of a Mass Tag Enables Direct Profiling of Active Matrix Metalloproteases

Lomane Berthy[1] | Ugo Pasco[2] | Mylene Sejalon-Cipolla[2] | Pierrick Bruyat[1] | Monika Kaminska[1] | Carole Malgorn[1] | Fabrice Beau[1] | Manca Osolin[3] | Metka Novak[3,4] | Barbara Breznik[3,4] | Dimitris Georgiadis[5] | Isabelle Correia[6] | Emeline Groult[7] | Olivier Lequin[6] | Sarah Bregant[1] | Yves-Marie Pers[7] | Daniele Noel[7] | Robert Thai[1] | Gilles Subra[2] | Sonia Cantel[2] | Laurent Devel[1]

[1]CEA, INRAE, Médicaments et Technologies pour La Santé (MTS), SIMoS, Université Paris-Saclay, Gif-sur-Yvette, France | [2]IBMM, Univ. Montpellier, ENSCM, CNRS, Montpellier, France | [3]National Institute of Biology, Department of Genetic Toxicology and Cancer Biology, 121 Večna pot, Ljubljana, Slovenia | [4]University of Ljubljana, Biotechnical Faculty, Ljubljana, Slovenia | [5]Department of Chemistry, Laboratory of Organic Chemistry, University of Athens, Panepistimiopolis, Zografou, Athens, Greece | [6]Sorbonne Université, Ecole Normale Supérieure, PSL University, CNRS, Chimie Physique, et Chimie du Vivant, CPCV, Paris, France | [7]IRMB, University of Montpellier, INSERM, CHU, Montpellier, France

Correspondence: Gilles Subra (gilles.subra@umontpellier.fr) | Sonia Cantel (sonia.cantel@umontpellier.fr) | Laurent Devel (Laurent.DEVEL@cea.fr)

Received: 21 October 2025 | **Revised:** 11 March 2026 | **Accepted:** 18 March 2026

Keywords: activity-based probes | chemoproteomic | mass tag | proximity-induced labeling

ABSTRACT

Conventional activity-based probes in activity-based protein profiling (ABPP) require enrichment or reporter tags for detection, which limits sensitivity and multiplexing. Here, we present an enrichment-free chemoproteomic approach that enables direct mass spectrometric detection by Matrix-Assisted Laser Desorption/Ionization (MALDI) of active proteases. An active-site–directed affinity probe transfers, through a proximity-induced reaction, a MALDI-detectable α-cyano-4-hydroxycinnamic acid (CHCA) tag exclusively to catalytically active forms of matrix metalloproteases (MMPs). The CHCA label enhances ionization efficiency and markedly improves signal-to-noise ratios, allowing confident identification of CHCA-labelled peptides under discriminating analytical conditions. Each active metalloprotease is thereby, associated with a distinct set of CHCA signature peptides, defining its activity fingerprint. This workflow achieves multiplexed and quantitative activity profiling of MMPs, directly in complex proteomes. This design expands ABPP into the mass spectrometry domain and establishes a robust platform for activity-based enzyme detection.

1 | Introduction

Proteases regulate nearly every aspect of protein homeostasis. At some point in their lifecycle, most proteins encounter a protease, leading to irreversible posttranslational modifications that modulate function, localization, or stability. Such events include secretion, activation via pro-peptide cleavage, membrane shedding, or degradation, underscoring the multifaceted roles of proteases in physiology and disease [1–4]. Among these enzymes, which together represent about 3% of the human genome, MMPs

Abbreviations: ABP, Activity-Based Probe; ABPP, Activity-Based Protein Profiling,; AfBP, Affinity-Based Probe; APMA, 4-Aminophenylmercuric Acetate (MMP activator); BB, Dibromo Phenyl Benzoate (cleavable linker); Bn, Benzyl spacer; CHCA, α-Cyano-4-hydroxycinnamic acid (mass tag and MALDI matrix); CHCE, α-cyano-4-hydroxycinnamic acid methyl ester (alternative MALDI matrix); Cy3, Cyanine 3 fluorescent dye; D-, Deuterated peptide analogue (internal standard); ECM, Extracellular Matrix; ELISA, Enzyme-Linked Immunosorbent Assay; ESI-MS, Electrospray Ionization Mass Spectrometry; LC-MS, Liquid Chromatography-Mass Spectrometry; MALDI, Matrix-Assisted Laser Desorption/Ionization; MMP, Human Matrix Metalloprotease; MS/MS, Tandem Mass Spectrometry; NASA, N-Acyl-N-Alkyl Sulphonamide (cleavable linker); PDB, Protein Data Bank; SI, Supporting Information; t½, Half-life; Tris, Tris(hydroxymethyl)aminomethane buffer..

Lomane Berthy, Ugo Pasco, and Mylene Sejalon-Cipolla contributed equally to this work.

In memory of Pr. Andrée Marquet

constitute a prominent subfamily of 23 zinc-dependent endopeptidases [5]. MMPs mediate tissue remodeling, cell signaling, and immune regulation, and are implicated in pathological contexts such as cancer [2, 6] and inflammatory disorders [5, 7, 8]. Secreted as latent zymogens, they are activated in the pericellular or extracellular space [9] to process a broad range of substrates, including extracellular matrix (ECM) and non-ECM proteins, thereby shaping tissue architecture and cellular dynamics [5, 10]. Under physiological conditions, MMP activity is tightly regulated by endogenous inhibitors, but this balance frequently collapses in disease, leading to uncontrolled proteolysis. Because MMPs can also activate one another and initiate proteolytic cascades [5, 10] monitoring their activation profiles in complex biological systems is essential for understanding their roles in health and pathology.

ABPP has emerged as a powerful means to interrogate enzymes in their functional state within complex proteomes [11]. This approach relies on activity-based probes (ABPs) that covalently label catalytically active enzymes through reactive warheads, enabling their identification and quantification [11–16]. For metalloproteases, which lack catalytic nucleophiles, photoreactive affinity-based probes (photo A*f*BPs) were introduced [11, 17], incorporating (i) an active-site recognition element, (ii) a photoreactive group that crosslinks upon UV irradiation, and (iii) an analytical tag. Such probes have enabled multiplexed profiling of metalloproteases in diverse biological systems [18–20]. However, these strategies rely on enrichment workflows (e.g., biotin-streptavidin pull-down or cleavable linker strategies [21]) prior to mass spectrometric analysis. Although effective, these additional steps increase the complexity of the analytical workflow and may introduce potential sources of variability, particularly when analyzing low-abundance proteases.

Inspired by affinity-guided protein conjugation strategies [22–25], we previously redesigned MMP-directed A*f*BPs by replacing photoreactive groups with electrophilic, cleavable linkers capable of proximity-driven acylation [26–28]. These linkers, such as acyl imidazole and N-acyl-N-alkyl sulphonamide (NASA) moieties, facilitate covalent transfer of fluorescent, clickable, or biotin-based handles to active MMPs without requiring photoactivation.

Building on this concept, we now introduce a photoactivation-free, mass-encoded ABPP strategy in which a transferable mass tag provides both selectivity and analytical readout. In this design, CHCA functions as a transferable mass tag that, in combination with a α-cyano-4-hydroxycinnamic acid methyl ester (CHCE) matrix, markedly enhances the signal-to-noise ratio of CHCA-labelled peptides while significantly reducing signals from non-labelled peptides under MALDI conditions [29, 30]. Upon digestion, CHCA-labelled metalloproteases yield distinctive CHCA signature peptides that reveal both enzyme identity and labelling site, enabling multiplexed detection, inhibitor profiling, and quantitative analysis of native MMPs secreted by cells (Figure 1A). Furthermore, through a deconvolution process combining a dedicated in-house bioinformatic tool with targeted MALDI-MS and MS/MS experiments, our approach enables the identification of additional active MMP targets beyond those initially anticipated from the probe design.

2 | Result and Discussion

2.1 | Assessment of Key Parameters Governing Labelling Efficiency and Selectivity

The A*f*BPs were designed to preferentially target lysine residues within the S_3' subsite of human MMPs (Figure S1). Each probe was built around a common phosphinic pseudopeptide recognition motif derived from a broad-spectrum MMP inhibitor [26], with a cleavable linker in its P_3' position (Figure 1B). To assess how geometry at this position as well as the intrinsic reactivity of cleavable linkers influence labelling efficiency and selectivity, two series of Cy3-labelled probes were first developed (Schemes S2, S4, S5, and Supplementary Methods). These probes incorporated either a NASA (**1-3-Cy3**) or a dibromo phenyl benzoate (BB) (**4-5-Cy3**) linker. These linkers preferentially react with lysine residues to form a peptide bond, with however a markedly different reactivity [22, 24]. The geometry at the P_3' position was modulated by varying the side-chain length and configuration, while the spacer between the cleavable linker and analytical handle consisted of either an alkyl chain (Alk; probes **1-4**) or a benzyl group (Bn; probe **5**), thereby tuning steric hindrance near the electrophilic center. Stability assays revealed rapid hydrolysis of the NASA-linked probe **1-Cy3** ($t½ \approx 3$ h), whereas the BB-linked analogue **5-Cy3** remained fully stable throughout the analysis (Figure S2), consistent with the difference of electrophilicity between the two linkers. All Cy3 probes displayed efficient binding to recombinant MMPs, with affinities ranging from tens to hundreds of nanomolar, indicating that target engagement is primarily driven by the shared recognition motif (Table S1). Labelling experiments (Figure S3) further showed that variations in P_3' geometry and nature of the spacer (Alk vs Bn) only weakly influenced probe reactivity (Figures S3C and S3D, respectively), whereas cleavable linker chemistry was the main determinant of selectivity. Thus, NASA-based **1-Cy3** probe exhibited broad labelling across several MMPs (Figure S3B), while BB-based **5-Cy3** probe showed near-exclusive reactivity toward MMP-12 (Figure S3E). Importantly, control experiments demonstrated that the reactive NASA probe **1-Cy3**, even at micromolar concentration, did not react with inactive zymogens of MMP-2, -9, -12, or -13 (Figure S4A), confirming its strict active-site-directed reactivity and the absence of allosteric activation under these conditions [9]. We further demonstrated that efficient labelling of MMP-2, -9, -12, and -13 can already be achieved within 1 h using **1-Cy3** (Figure S4B). However, because a systematically higher labelling efficiency is observed after 4 h for all four MMPs, this incubation time was selected to ensure more complete and reproducible labelling.

Based on their labelling behaviors, namely broad reactivity across several MMPs for **1-Cy3** and near-selective labelling of MMP-12 for **5-Cy3**, these two probes were selected for conversion into CHCA-tagged analogues. Importantly, the resulting probes, **1-CHCA** and **5-CHCA** (Figure S1B), differ from their Cy3 counterparts only by the analytical handle (Cy3 versus CHCA) and

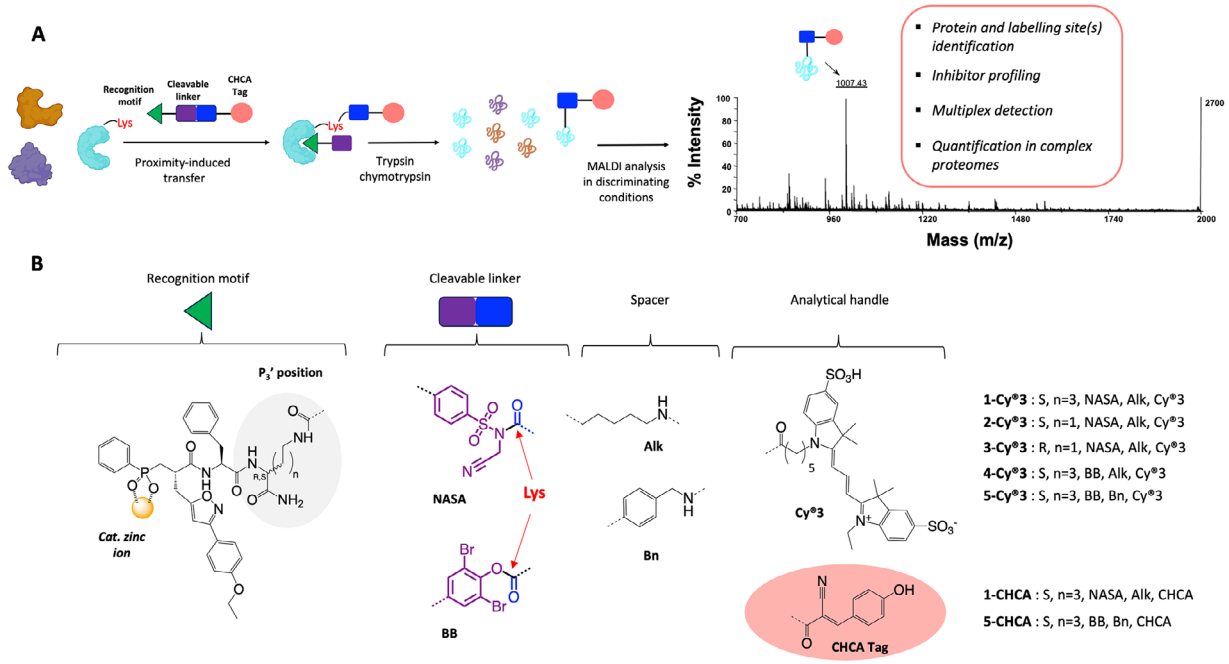

FIGURE 1 | Mass-encoded chemoproteomic strategy for metalloprotease profiling. (A) Schematic overview of the mass-encoded chemoproteomic workflow. The method enables the direct identification of labelled metalloproteases and precise mapping of covalent modification sites within a single experiment, while allowing inhibitor profiling, multiplexed detection, and quantitative analysis of proteases in complex proteomes. (B) Chemical structures of affinity-based probes (A*f*BPs) incorporating: (i) a phosphinic pseudopeptide core targeting the metalloprotease active site; (ii) a cleavable linker, either N-acyl-N-alkyl sulphonamide (NASA; probes **1**–**4**) or dibromo phenyl benzoate (BB; probes **5**); and (iii) an analytical handle, consisting of a fluorescent dye (Cy3) for in-gel fluorescence imaging or a mass tag (α-cyano-4-hydroxycinnamic acid, CHCA) for mass-encoded analysis. The handle is connected via either an alkyl (Alk; probes **1**–**4**) or benzyl (Bn; probes **5**) spacer.

retain comparable binding affinity and selectivity profiles toward MMPs (Tables S1 and S2).

2.2 | Determination of CHCA Signature Peptides of MMP-2, 9, 12, and 13 and Their Respective Labelled Residues

The **1-CHCA** probe (1 μM) was evaluated on human MMP-2, -9, -12, and -13 (50 nM each) in Tris buffer (50 mM, 10 mM $CaCl_2$, 50 μM $ZnCl_2$, 0.01% Brij 35, pH 7.4) at 37°C for 4 h. Under identical conditions, the **5-CHCA** probe (1 μM) was tested on MMP-12. On the basis of the inhibitory constants (Table S1), which govern equilibrium complex formation between the probes and the MMPs, a concentration of 1 μM was selected to ensure near-complete active-site occupancy (>99%) of MMP-2, -9, -12, and -13 under the experimental conditions used.

After heat denaturation and acetone precipitation, CHCA-labelled MMPs were digested (chymotrypsin for MMP-9, -12, and -13; sequential trypsin/chymotrypsin for MMP-2), desalted, and analyzed by MALDI-TOF using CHCA and CHCE matrices (Figures S5–S8).

As previously reported the combination of a CHCE matrix with a CHCA mass tag markedly improves the signal-to-noise ratio of CHCA-labelled peptides while strongly suppressing signals from non-labelled peptides [29, 30]. In this respect, CHCE acts as a discriminating matrix, favoring the selective detection of CHCA-tagged species. Differential analysis of MMP-2 digests revealed a peak at *m/z* 1007.4 (and its oxidized form at *m/z* 1023.4), preferentially detected under CHCE conditions (Figure 2A). MS/MS sequencing identified this signal as a CHCA-tagged signature peptide, characterized by a diagnostic fragment ion at *m/z* 368.2 (Figure 2B), likely corresponding to a CHCA-Alk-Lys immonium ion (Figure S9) [31], with labelling assigned to Lys^{372} within the fibronectin insert in the S_3' region of MMP-2 (Figure 2C, left panel). Similarly, signature peptides at *m/z* 1543.9 (MMP-9) and 1369.7 (MMP-12) were identified, corresponding to CHCA-labelled Lys^{214} and Lys^{177}, respectively (Figure 2C, center panels; Figures S10–S11), both located within the catalytic S_3' subsite. Upon treatment of MMP-12 with **5-CHCA**, the same Lys^{177} residue was modified, yielding a peptide at *m/z* 1389.7 with a diagnostic ion at *m/z* 388.2 (Figures S11A–C). The 20 Da mass difference observed both in MS and MS/MS, reflects the substitution of the alkyl spacer in **1-CHCA** by a benzyl group in **5-CHCA** and further confirms CHCA-Lys immonium ion as a characteristic diagnostic ion. When comparing the digest of **1-CHCA**-labelled MMP-12 with that of **5-CHCA**-labelled one, this difference of 20 Da in mass proved particularly useful to unambiguously identify additional CHCA-labelled peptides and their respective labelling sites, including Lys^{436} and Lys^{378}/Lys^{379} from the hemopexin-like domain and Lys^{111} from the catalytic domain (Figures S11D–F). These results indicate that, both probes can label MMP-12 transient intermediates retaining partial connectivity between their catalytic and hemopexin domain, despite a propensity for autolysis [32, 33] as observed during labelling experiments with Cy3 probes (Figure S3). They also align with the

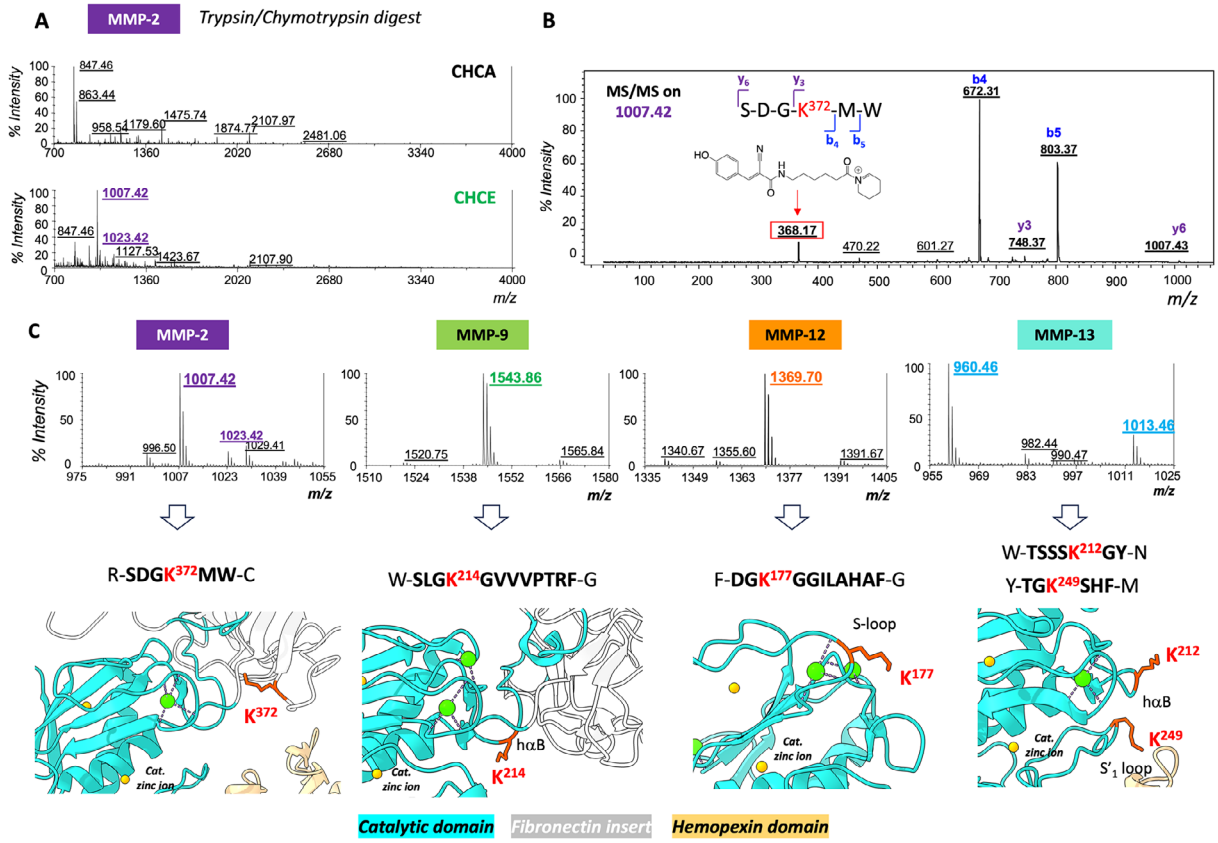

FIGURE 2 | Identification of CHCA-labelled signature peptides from MMPs (A) Differential MALDI-MS analysis of human MMP-2 digested with trypsin/chymotrypsin and analyzed in positive-ion mode using either CHCA (top) or CHCE (bottom) matrices. A peak at *m/z* 1007.4 and its oxidized form at *m/z* 1023.4, preferentially observed under CHCE conditions, are highlighted in purple. (B) MS/MS spectrum of the *m/z* 1007.4 peptide acquired under CHCE conditions in positive-ion mode. The labelled lysine residue (Lys^{372}) is shown in red within the peptide sequence. Annotated b- and y-type fragment ions are indicated in blue and purple, respectively, and the diagnostic CHCA fragment ion at *m/z* 368.2 is boxed in red. (C) CHCA-labelled signature peptides mapped onto the catalytic domains of human MMP-2, -9, -12, and -13 (PDB IDs: 1CK7, 1L6J, 3LIK, and 4FU4). Lysine residues identified as CHCA-labelled from peptide MS/MS spectra are displayed as red sticks. Structural domains are color-coded: catalytic domain (cyan), fibronectin-like domain (light grey), and hemopexin domain (orange). Zinc (yellow) and calcium (green) ions are shown as spheres.

high conformational mobility of MMP-12 catalytic domain [34], which enables labelling of Lys^{111} at the N-terminal end despite the cleavable linker being projected toward the opposite subsite (Figure S11H). For MMP-13, two characteristic CHCA signature peptides at *m/z* 960.4 and 1013.4, corresponding to labelling of Lys^{249} and Lys^{212} within the S_3' subsite, were identified (Figure 2C, right panel; Figure S12). Noteworthy, in all CHCA-Alk-labelled peptides, the diagnostic fragment ion at 368.2 was consistently observed (Figures S10–S12). Finally, competition experiments with the active-site inhibitor RXP500.1 (10 μM) strongly reduced CHCA labelling (Figures S5–S8), confirming both the specificity of the labelling and the active-site-directed reactivity of **1-CHCA** and **5-CHCA** probes.

2.3 | Selectivity of A*f*BP With BB Cleavable Linker

The clear identification of reactive lysine residues within the S_3' subsite of MMP-2, -9, -12, and -13 prompted further investigation into the exceptional selectivity of the BB probes for MMP-12. Specifically, we sought to understand why MMP-2 and MMP-9 exhibited poor reactivity toward this probe, despite sharing a lysine residue (Lys^{187} in MMP-2 and Lys^{184} in MMP-9) with MMP-12 (Lys^{177}) within their respective S-loops (Figure S13A). Interestingly, substituting Asp^{185} with Gly^{185} in MMP-9 partially restored the reactivity of Lys^{184} toward **5-Cy3** (Figure S13B), whereas introducing the reverse mutation (Gly^{178}→Asp^{178}) in MMP-12 markedly reduced the reactivity of Lys^{177}. These findings indicate that the presence of an adjacent aspartate near the S-loop lysine in MMP-2 and MMP-9 substantially decreases its nucleophilicity. This observation is consistent with previous studies showing that the local microenvironment modulates the p*Ka* of lysine residues, thereby influencing their intrinsic reactivity when interacting with nearby carboxylate groups [35]. Furthermore, the BB-cleavable electrophile exhibited negligible reactivity toward MMP-2 Lys^{372}, MMP-9 Lys^{214}, or MMP-13 Lys^{212} and Lys^{249}, as reflected by the low signal-to-noise detection of CHCA signature peptides indicative of covalent modification by the **5-CHCA** probe (data not shown). These results suggest that MMP-12 Lys^{177}, preferentially targeted by both **1-CHCA** and **5-CHCA** (Figures S7 and S11), is not only significantly more reactive than MMP-2 Lys^{187} and MMP-9 Lys^{184}, but also optimally positioned to engage with a cleavable linker, even one of limited intrinsic reactivity.

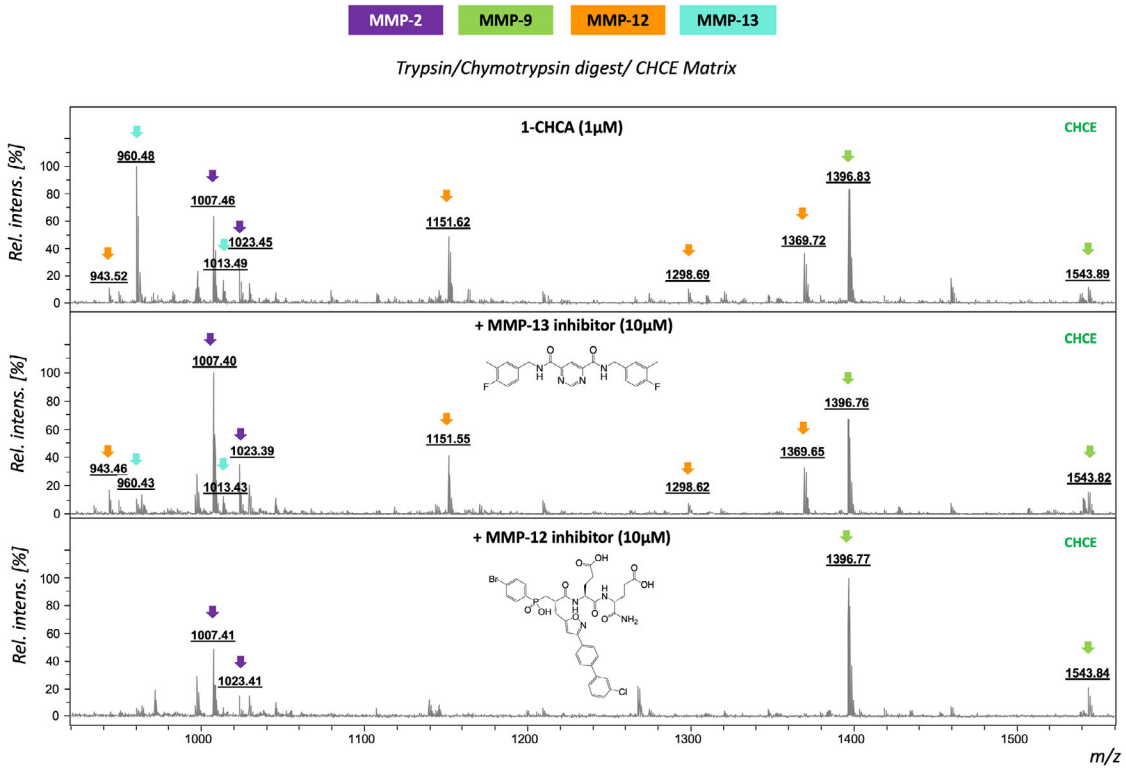

FIGURE 3 | Multiplexed detection of CHCA-labelled MMP signature peptides and modulation of activity-dependent CHCA-labelled peptides upon inhibitors incubation. Human MMP-2, -9, -12, and -13 (10 nM) was incubated as a mixture with probe **1-CHCA** (1 µM, 4 h, 37 °C) either alone (top) or after preincubation (30 min) with a selective inhibitor of MMP-13 (middle) or MMP-12 (bottom) at 10 µM. Samples were digested with trypsin/chymotrypsin and MALDI analysis were performed under CHCE matrix conditions. Signature peptides corresponding to each MMP are indicated by colored arrows: MMP-2 (purple), MMP-9 (green), MMP-12 (orange), and MMP-13 (cyan).

2.4 | Multiplexed Detection of MMPs and Modulation of Activity-Dependent CHCA-Labelled Peptides Upon Inhibitor Incubation

A labelling experiment was performed on a mixture of four human MMPs (MMP-2, -9, -12, and -13, each at 10 nM) incubated with the broad-spectrum **1-CHCA** probe (1 µM) at 37°C for 4 h. Following proteolytic digestion with a combination of trypsin and chymotrypsin, the resulting CHCA-labelled and unlabelled peptide mixtures were analyzed under CHCE-discriminating conditions (Figure 3, upper panel). Under these conditions, CHCA signature peptides corresponding to MMP-2 (*m/z* 1007.4 and 1023.4, purple arrow), MMP-9 (*m/z* 1396.8 and its partially processed variant at 1543.8, green arrow), MMP-12 (*m/z* 1369.7 and related peptides at 1298.7, 1151.6, and 943.4 resulting from missed cleavages, orange arrow), and MMP-13 (*m/z* 960.4 and 1013.4, blue arrow) were unambiguously detected.

This multiplexed detection of MMPs enables the rapid and qualitative assessment of inhibitor selectivity within a single experimental workflow. To demonstrate this, we evaluated the ability of active-site-directed MMP inhibitors to compete with **1-CHCA** for binding to MMP-2, -9, -12, and -13. The presence or disappearance of CHCA-labelled peptide signals served as a qualitative indicator of enzyme activity or inhibition, enabling rapid screening of enzymatic modulation under the experimental conditions, without the need for precise quantitative measurements.

Preincubation of a highly selective MMP-13 inhibitor [36] (10 µM) with the four MMPs for 30 min prior to **1-CHCA** labelling (1 µM) resulted in a decrease in intensity of MMP-13 signature peptides, while those of MMP-2, -9, and -12 remained detectable (Figure 3, central panel). Under these conditions, the MMP-13 inhibitor retained full selectivity toward MMP-13, sparing the other MMPs. In a separate experiment, the phosphinic pseudopeptide RXP470.1, a selective MMP-12 inhibitor [37], was incubated (10 µM, 30 min) with the same MMP mixture before **1-CHCA** labelling (1 µM) (Figure 3, lower panel). Blocking the MMP active site with RXP470.1 resulted not only in the disappearance of CHCA signature peptides from MMP-12, but also affected those of MMP-13 and, to a lesser extent, MMP-2. This observation indicates that the selectivity of RXP470.1 for MMP-12 decreases at 10 µM, consistent with its inhibition constants for MMP-2, -12, and -13 (Table S1).

By coupling catalytic activity to protease-specific mass signatures, the method allows simultaneous monitoring of multiple targets present at nanomolar concentration, without enrichment or gel-based analyses. In addition, competition experiments with inhibitors provide a rapid readout of inhibitor selectivity, with an activity-dependent signal suppression directly visualized in the mass spectra. This approach, complementary to established ABPP-based multiplexing strategies for evaluating target engagement [38], offers a simplified analytical workflow based on direct MALDI detection and identification. Although, the present study emphasizes qualitative activity readouts, this

analytical framework offers clear potential for extension to dose-response analyses under appropriately standardized conditions, as demonstrated in previous CHCA-based MALDI competitive assays [30].

2.5 | Detection and Quantification of MMPs in Complex Proteomes and Cell Supernatants

To evaluate the performance of our workflow to quantify active forms of MMP, recombinant MMP-13 (10 nM), alone or spiked into 40 µL of mouse breast tumor extract at 125 µg/mL. In this last case, MMP-13 (0.02 µg, 400 fmol) corresponded to 0.4% of total proteome and was labelled with **1-CHCA** (1 µM) at 37° C for 4 h (Figure S14). The samples were then subjected to the complete workflow, including precipitation, dual trypsin/chymotrypsin digestion, desalting, and MALDI analysis under CHCE conditions.

For absolute quantification, heavy deuterated analogues of the two CHCA signature peptides (*m/z* 960.4 and 1013.4, Figure S14A) were synthesized and added during MALDI analysis as internal standards for calibration (Figure S14B). When recombinant MMP-13 alone was processed through the entire workflow, the CHCA-labelled peptides at *m/z* 960.4 and 1013.4 were quantified at 31.1 ± 6.1 and 26.0 ± 3.6 fmol, respectively (Figure S14C). The 57.1 fmol detected, relative to the initial 400 fmol present in the sample, corresponded to an overall detection yield of 14% ± 2%. This calculation assumes stoichiometric mass-tag transfer, namely the transfer of a single CHCA tag per enzyme molecule, as previously demonstrated for reactive probes incorporating a phosphinic pseudopeptide scaffold [26].

In the tumor extract, after labelling and verification of complete trypsin/chymotrypsin digestion by electrophoresis (Figure S14D), both signature peptides from MMP-13 were unambiguously detected (Figure S14E). In this case, CHCA-labelled peptides at *m/z* 960.4 and 1013.4 were quantified at 7.2 ± 0.9 and 13.8 ± 3.3 fmol, respectively. The total amount of CHCA-labelled peptides (21 fmol) corresponded to a detection yield of 5.3% ± 0.9%, relative to the 400 fmol spiked into the mouse extract, and to an estimated MMP-13 concentration of approximately 0.5 nM. (Figure S14F). This underestimation may partly result from probe consumption through non-specific reactions with abundant proteins such as serum albumin, as evidenced by the detection of CHCA-modified albumin peptides at *m/z* 1072.5 (Figures S14E, G, and H), consistent with previous observations for NASA-linked AfBPs [26].

The same quantitative workflow was then applied to detect and measure active MMPs secreted by cells. The supernatant of HEK293T cells expressing pro-mMMP-12 [27] was first activated with APMA, and engagement of the **5-CHCA** probe (1 µM) with activated mMMP-12 was verified through an enzyme assay (Figure S15A). After four hours at 37°C, the proteome was analyzed using our workflow, including dual trypsin/chymotrypsin digestion. Under CHCE conditions, a peak at *m/z* 951.4 (Figure S15B) was preferentially detected. This signature peptide corresponded to the covalent modification of Lys^{181} by the benzyl-CHCA tag within the S_3' subsite of mMMP-12, as confirmed by its MS/MS fragmentation pattern and the presence of the diagnostic fragment ion at *m/z* 388.2 (Figures S15C and D). Using a deuterated standard peptide (D-951-mMMP-12) for calibration, the concentration of active mMMP-12 in the supernatant was determined to be 9.4 nM (Figures S15E and F). Notably, this measurement very closely matches values obtained by standard enrichment and on-bead digestion methods followed by ESI-MS targeted mass spectrometry [27]. This demonstrates that our CHCA workflow enables accurate and direct quantification of the active enzyme without additional purification steps.

Similarly, we evaluated the ability of probe **1-CHCA** to detect and quantify endogenous MMP-2 in the supernatant of U87 glioblastoma cells [39]. Its presence and concentration (40 nM, corresponding to 0.2% of the total proteome) were confirmed by Western blot analysis (Figure S16A) and ELISA, respectively. Notably, both Western blot analysis and an MMP-directed fluorogenic substrate assay (Figure S16B) suggested that MMP-2 was present predominantly in its inactive (pro-MMP-2) form in this supernatant. After APMA activation (1 mM, 1 h, 37 °C), a well-established reagent used to activate pro-MMPs via disruption of the cysteine switch mechanism [40], **1-CHCA** labelling (1 µM) was performed (4 h at 37 °C) followed by dual trypsin/chymotrypsin digestion. The resulting digest was analyzed both under CHCE-discriminating conditions and under standard MALDI conditions using conventional CHCA matrix (Figure S16C), further illustrating the ability of CHCE conditions to selectively reduce signals from unlabelled peptide fragments (Figure S16C, lower panel). Notably, under CHCE-discriminating conditions, a CHCA-tagged MMP-2 peptide (*m/z* 1007.4) was clearly detected, consistent with labelling of the active enzyme, whereas no corresponding signal was observed in non-activated or inhibitor-treated samples (Figure 4A, B). Quantification using the D-1007-MMP-2 (Figure S16D) standard yielded an active MMP-2 concentration of 20 ± 1 nM (Figure 4C), in good agreement with the total MMP-2 concentration measured by ELISA. Two additional peaks (*m/z* 1001.7 and 1045.7; Figure 4A) were detected both in the non-activated sample and in the sample preincubated with a broad-spectrum MMP inhibitor. MS/MS experiments did not indicate any of CHCA conjugation, nor confident assignment of the corresponding peptide sequences. These signals therefore most likely arise from background species and are not associated with probe-mediated labelling of active metalloproteases.

An additional CHCA-labelled albumin peptide (*m/z* 1101.6) was consistently detected, further confirming albumin as a recurrent off-target of **1-CHCA** (Figure 4A–D). Moreover, identification of Lys^{455} as a preferential labelling site suggests a potential binding pocket for **1-CHCA** near site II of serum albumin (Figure 4D) [41]. This site is known to bind aromatic derivatives carrying negative charges, consistent with the chemical structure of **1-CHCA**.

2.6 | Detection of Active MMP-3 in Human Chondrocyte Supernatants

We next applied our chemoproteomic workflow to profile metalloproteases secreted by primary human chondrocytes stimulated with IL-1β, a pro-inflammatory cytokine known to induce the expression and release of MMPs in this cellular context [42]. Chondrocytes were isolated from the femoral condyles of

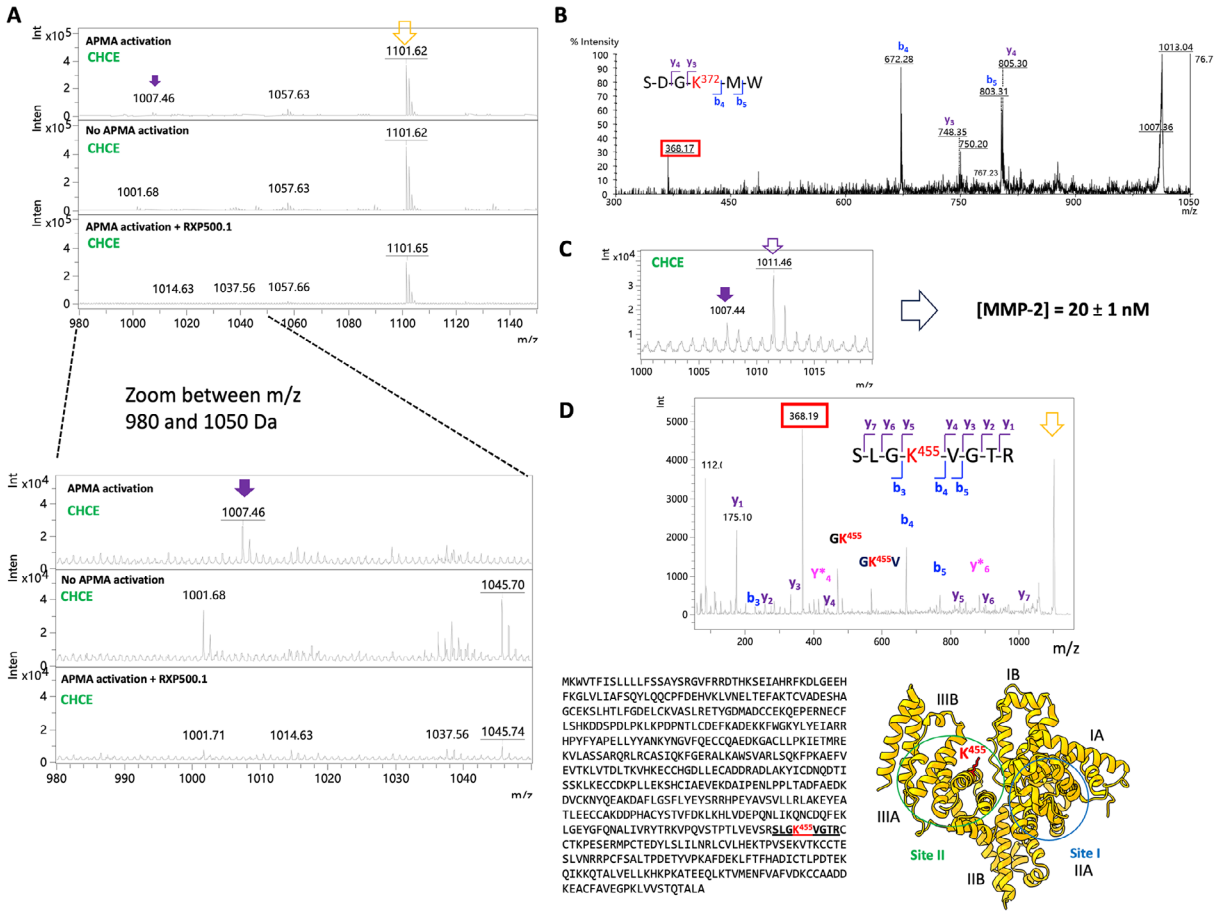

FIGURE 4 | Detection and quantification of activated MMP-2 in the U87 glioblastoma cell secretome. (A) MALDI mass spectra of U87 cell supernatants labelled with **1-CHCA** (1 μM, 4 h, 37 °C) and digested with trypsin/chymotrypsin. Samples were either APMA-activated (1 mM, 1 h, 37 °C; top), non-activated (middle), or APMA-activated followed by incubation with the inhibitor RXP500.1 (bottom). Analyses were performed under CHCE matrix conditions. The MMP-2 signature peptide at *m/z* 1007.4 is indicated by a purple arrow; a background peptide at *m/z* 1101.6, present under all conditions, is marked in yellow. (B) MS/MS spectrum of the *m/z* 1007.4 peptide acquired under CHCE conditions. The CHCA-labelled lysine (Lys^{372}) is shown in red. Annotated b- and y-type fragment ions are colored blue and purple, respectively, and the diagnostic CHCA fragment ion at *m/z* 368.2 is boxed in red. (C) MALDI-MS spectrum (*m/z* 1000–1020) of APMA-activated U87 supernatant labelled with **1-CHCA** in the presence of a deuterated MMP-2 reference peptide (D-1007-MMP-2). Quantification yielded an estimated MMP-2 concentration of 20 ± 1 nM (mean ± SD, $n = 3$). (D) MS/MS spectrum of the peptide at *m/z* 1101.6 acquired under CHCE conditions. The labelled lysine (Lys^{455}) is highlighted in red. Annotated b- and y-type ions are colored blue and purple, and the CHCA-specific fragment ion at *m/z* 368.2 is boxed in red. The structure of bovine serum albumin (BSA, PDB: 4OR0) is shown with domains I–III and subdomains A and B indicated. The approximate positions of sites I and II are marked with blue and green circles, respectively. The protein core is shown as a yellow cartoon, and Lys^{455} near site II is displayed as a red stick. The corresponding peptide sequence highlights Lys^{455} in red.

osteoarthritic patients ($n = 5$; Figure 5A), mixed, cultured for 24 h with or without IL-1β, and the resulting supernatant reacted overnight with probe **1-CHCA**. Importantly, no pre activation with APMA was performed in this case. MALDI analysis revealed a CHCE-specific signal at *m/z* 1385.7 detected only in IL-1β-treated samples (Figure 5A), whereas a *m/z* 1101.6 peak was common to all samples and attributed to serum albumin labelling.

To annotate CHCA-labelled peptides, we developed Enzymator (https://github.com/ugo351/enzymator.git), a differential spectral analysis tool that deconvolutes CHCA-modified peptides by comparing experimental and theoretical *m/z* values derived from MMP, ADAMTS, and albumin sequences. Peaks displaying the diagnostic 368.2 fragment were validated by MS/MS and matched against theoretical spectra generated by Protein Prospector and Enzymator (See supplementary methods for further details). Validation using recombinant MMPs confirmed accurate peptide assignment (e.g., CHCA-labelled MMP-13 at *m/z* 960.4; Figure S17).

We then applied a three-step deconvolution strategy to assign the signal at *m/z* 1385.7. First, the MS profile of the trypsin/chymotrypsin digest from IL-1β-stimulated chondrocytes analyzed under CHCE matrix conditions was compared with that obtained using a standard CHCA matrix (Figure S18A), confirming that the *m/z* 1385.7 signal is preferentially detected under CHCE-discriminating conditions. This ion was subsequently subjected to MS/MS fragmentation (Figure S18B). The resulting fragmentation pattern revealed the presence of the diagnostic CHCA-derived fragment ion at *m/z* 368.2, thereby confirming conjugation of the peptide to the CHCA mass tag (Figure 5B). In a second step, the experimental MS/MS

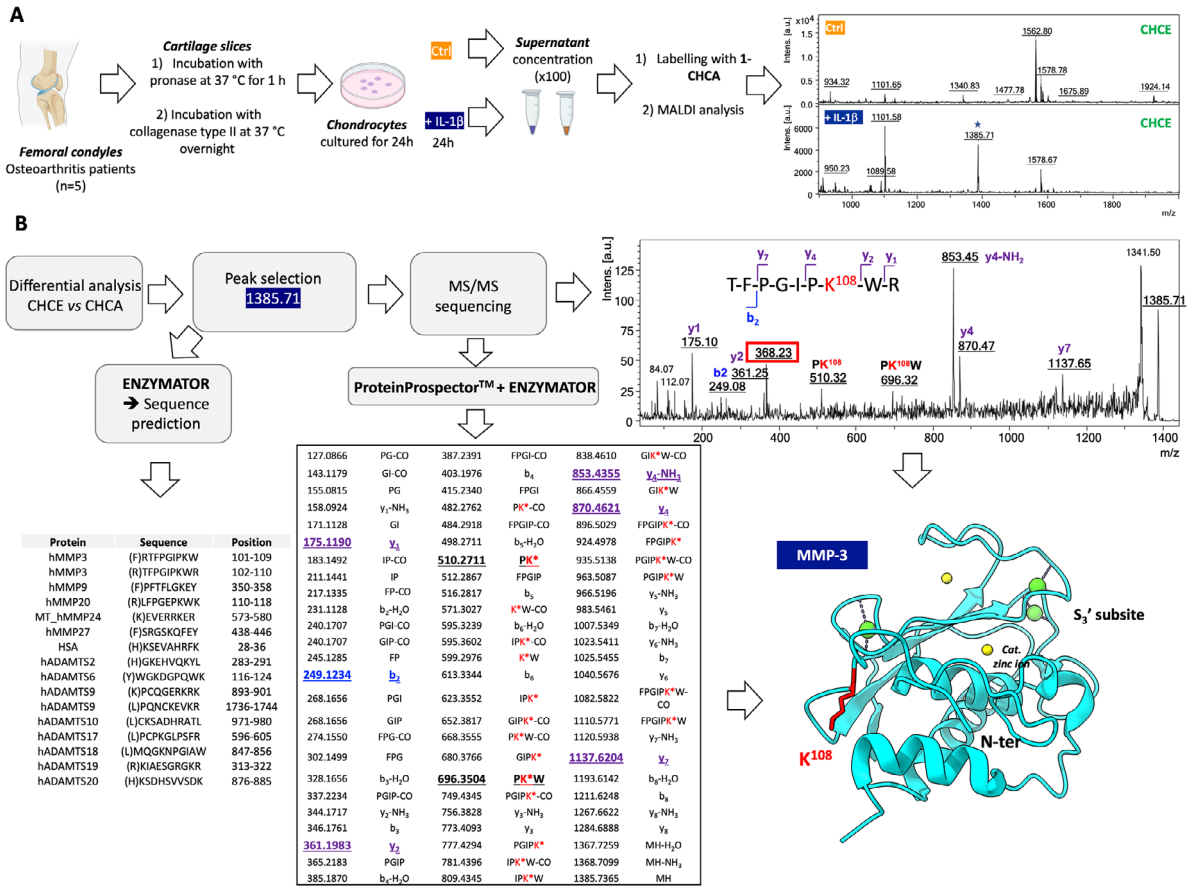

Protein	Sequence	Position
hMMP3	(F)RTFPGIPKW	101-109
hMMP3	(R)TFPGIPKWR	102-110
hMMP9	(F)PFTFLGKEY	350-358
hMMP20	(R)LFPGEPKWK	110-118
MT_hMMP24	(K)EVERRKER	573-580
hMMP27	(F)SRGSKQFEY	438-446
HSA	(H)KSEVAHRFK	28-36
hADAMTS2	(H)GKEHVQKYL	283-291
hADAMTS6	(Y)WGKDGPQWK	116-124
hADAMTS9	(K)PCQGERKRK	893-901
hADAMTS9	(L)PQNCKEVKR	1736-1744
hADAMTS10	(L)CKSADHRATL	971-980
hADAMTS17	(L)PCPKGLPSFR	596-605
hADAMTS18	(L)MQGKNPGIAW	847-856
hADAMTS19	(R)KIAESGRGKR	313-322
hADAMTS20	(H)KSDHSVVSDK	876-885

127.0866	PG-CO	387.2391	FPGI-CO	838.4610	GIK*W-CO
143.1179	GI-CO	403.1976	b_4	853.4355	y_4-NH_3
155.0815	PG	415.2340	FPGI	866.4559	GIK*W
158.0924	y_1-NH_3	482.2762	PK*-CO	870.4621	y_4
171.1128	GI	484.2918	FPGIP-CO	896.5029	FPGIPK*-CO
175.1190	y_1	498.2711	b_5-H_2O	924.4978	FPGIPK*
183.1492	IP-CO	510.2711	PK*	935.5138	PGIPK*W-CO
211.1441	IP	512.2867	FPGIP	963.5087	PGIPK*W
217.1335	FP-CO	516.2817	b_5	966.5196	y_5-NH_3
231.1128	b_2-H_2O	571.3027	K*W-CO	983.5461	y_5
240.1707	PGI-CO	595.3239	b_6-H_2O	1007.5349	b_7-H_2O
240.1707	GIP-CO	595.3602	IPK*-CO	1023.5411	y_6-NH_3
245.1285	FP	599.2976	K*W	1025.5455	b_7
249.1234	b_2	613.3344	b_6	1040.5676	y_6
268.1656	PGI	623.3552	IPK*	1082.5822	FPGIPK*W-CO
268.1656	GIP	652.3817	GIPK*-CO	1110.5771	FPGIPK*W
274.1550	FPG-CO	668.3555	PK*W-CO	1120.5938	y_7-NH_3
302.1499	FPG	680.3766	GIPK*	1137.6204	y_7
328.1656	b_3-H_2O	696.3504	PK*W	1193.6142	b_8-H_2O
337.2234	PGIP-CO	749.4345	PGIPK*-CO	1211.6248	b_8
344.1717	y_2-NH_3	756.3828	y_3-NH_3	1267.6622	y_8-NH_3
346.1761	b_3	773.4093	y_3	1284.6888	y_8
361.1983	y_2	777.4294	PGIPK*	1367.7259	MH-H_2O
365.2183	PGIP	781.4396	IPK*W-CO	1368.7099	MH-NH_3
385.1870	b_4-H_2O	809.4345	IPK*W	1385.7365	MH

FIGURE 5 | Identification of MMP-3 in supernatants from primary human chondrocytes. (A) Experimental workflow. Primary chondrocytes were isolated from the femoral condyles of five patients with knee osteoarthritis (OA), cultured, and stimulated with IL-1β for 24 h. The resulting supernatants were concentrated and labelled overnight at room temperature with **1-CHCA** (1 µM). After trypsin/chymotrypsin digestion, samples were analyzed by MALDI–MS using the CHCE matrix. Representative spectra from one control (Ctrl, orange) and one IL-1β-treated sample (dark blue) are shown. A peak at 1385.7 Da, detected exclusively in the IL-1β-treated sample, is indicated by a blue star. (B) Workflow for deconvolution of CHCA-labelled peptides. Comparative MALDI–MS analyses using CHCA and CHCE matrices enabled identification of peaks selectively enriched under CHCE conditions. These peaks were further analyzed using Enzymator and validated by MS/MS sequencing, revealing a previously unannotated CHCA-labelled peptide corresponding to human MMP-3 in IL-1β-stimulated samples. The labelled lysine (Lys^{108}) is located in the S_3 subsite of the MMP-3 catalytic domain (PDB: 4G9L). The domain is shown in cyan, with zinc (yellow) and calcium (green) ions depicted as spheres, and the CHCA-labelled lysine highlighted as red sticks.

spectrum was compared with theoretical MS/MS spectra generated using Protein Prospector for the 15 candidate peptide sequences predicted by Enzymator (Figures 5B, S18C, and S18D). Comparison across all candidate peptides, together with the number of matching experimental MS/MS fragment ions for each sequence, identified the MMP-3 peptide (TFPGIPK*WR, labelled at Lys^{108}) as the highest-confidence assignment, with eight matching fragment ions (Figure S18C). Finally, to independently validate this assignment, recombinant MMP-3 was labelled with probe 1-CHCA, enabling confirmation of its MALDI-MS fingerprint under CHCE conditions (Figure S19A), as well as the corresponding MS/MS fragmentation pattern of the *m/z* 1385.7 signal (Figure S19B). The excellent agreement between the experimental and theoretical fragmentation patterns (Figure S19C) provides unambiguous confirmation of the assignment.

These findings are consistent with IL-1β-induced MMP-3 secretion by chondrocytes [43] and suggest a high degree of flexibility in the enzyme's N-terminal region, as previously observed for MMP-12.

2.7 | Probing MMP Activity Through Mass-Tag Transfer Chemistry

This work establishes a mass-encoded ABPP strategy in which a transferable mass tag provides both chemical selectivity and analytical readout. By coupling proximity-driven chemistry with MALDI-based detection, the approach integrates molecular recognition with MALDI mass spectrometric sensitivity, enabling rapid and quantitative analysis of catalytically active MMPs directly in complex proteomes. Each labelled enzyme yields a unique, or a defined panel of, CHCA-derived signature peptides that constitute an activity fingerprint, enabling multiplexed, and comparative analyses without enrichment.

The efficiency and quantitative accuracy of the workflow are governed by multiple parameters, including probe labelling efficiency, protein recovery, digestion completeness, and peptide extraction, each of which may be influenced by sample complexity. For instance, MMP-2 detection yields were higher in U87 cell supernatants (~50%) than in buffer (~18%; Figure S16E), whereas

more complex matrices, such as tumor extracts, resulted in reduced yields. These observations underscore the inherent challenges associated with absolute quantification of active MMPs across heterogeneous biological samples. Nevertheless, this limitation, also encountered with other quantification methods, does not preclude accurate measurement of endogenous active MMPs in three distinct proteomes examined in this study. In this respect, our strategy enables determination of active MMP concentrations with defined accuracy, precision, and linearity within samples of comparable complexity.

Although a direct one-to-one comparison with enrichment-based ABPP workflows is non-trivial due to fundamental differences in sample handling and readout, the close agreement between enrichment-based and enrichment-free quantification of activated mMMP-12 in HEK293T supernatants supports the accuracy and validity of the direct quantification achieved with the present method. In this regard, the principal advantage of our approach lies in direct, enrichment-free, mass-based quantification of catalytically active MMPs, rather than incremental gains in analytical sensitivity. Moreover, when combined with ELISA, an assay that measures total protein levels irrespective of activation state, this strategy enables estimation of the fraction of active MMPs within a given sample. This distinction is particularly relevant in light of growing evidence that MMP activity, rather than expression alone, correlates with disease progression and diagnostic value [2, 8, 44–46].

The applicability of this enrichment-free strategy depends on two key parameters: (i) efficient binding of A*f*BPs to the target enzyme, primarily dictated by the recognition motif, and (ii) the presence of a suitably positioned nucleophilic residue, such as a lysine, in proximity to the binding site to enable proximity-induced mass-tag transfer. In this context, A*f*BPs projecting a cleavable linker into the S_3' subsite preferentially label MMP-2, -9, -12, and -13, which contain lysine residues within this region. Notably, labelling of MMP-12, -3 in their S_3 subsite, likely facilitated by a higher degree of flexibility from their N-terminal region, illustrates the potential extensibility of this design principle to other MMPs and proteases. For MMPs, this may involve the development of CHCA-derived A*f*BPs targeting the S_3 subsite, which contains a reactive N-terminus and multiple lysine residues [28]. For other protease families, broader applicability will likely require libraries of probes incorporating distinct recognition motifs and cleavable linkers with varied reactivity and projection geometries. In addition, targeting alternative nucleophilic residues within the catalytic cleft may further expand the scope of this bioanalytical strategy. Collectively, these developments define important directions for future CHCA-derived probe design, with the perspective of comprehensive mapping of protease activation patterns across physiological and pathological contexts.

Within the scope of the present study, MALDI analysis coupled with MS/MS sequencing identified serum albumin as the principal off-target of the A*f*BPs. This observation can be attributed to the high abundance of albumin in biological samples, together with the hydrophobic scaffold and negatively charged features of the probes. While the present approach is quantification-oriented rather than discovery-driven, this result nonetheless suggests that mass-tag transfer combined with deconvolution strategies could support probe-based target identification under appropriate conditions [16, 47].

Beyond profiling MMP activity in liquid samples, the intrinsic MALDI compatibility of the CHCA tag suggests that, this strategy could be extended to mass spectrometry imaging, enabling spatially resolved mapping of MMP activity in tissues. Such developments could help bridge chemical proteomics and diagnostic mass spectrometry, ultimately facilitating the identification of mass-encoded activity biomarkers and advancing translational applications of ABPP.

Overall, by validating proximity-induced mass-tag transfer as a robust analytical principle, this work establishes a generalizable framework for CHCA-derived probe design. The CHCA tag provides an orthogonal, MALDI-compatible readout, offering a scalable and multiplexable platform for investigating enzyme activity in native biological environments [48].

3 | Conclusion

We have developed a new generation of affinity-based probes that enable the proximity-induced transfer of a MALDI-detectable mass tag selectively to catalytically active MMPs, allowing their direct identification and quantification without enrichment. This strategy extends ABPP into the mass spectrometry domain by translating enzyme activity into a mass-encoded analytical readout. The approach provides sensitive, multiplexed, and quantitative detection of active MMPs in complex proteomes. By combining chemical selectivity with analytical simplicity, this work establishes a general design principle that can be adapted to other metalloprotease and enzyme families and may enable functional biomarker discovery in physiological and pathological contexts.

4 | Supporting Information

The Supporting Information includes Figures S1–S19, Schemes S1–S5, Tables S1–S5, supplementary methods, and NMR and HPLC data of the chemical probes and their synthetic precursors.

Acknowledgments

This work was supported by the French National Research Agency (ANR-18-CE44-0012 and ANR-24-CE44-0275). This work was also supported by the Slovenian Research and Innovation Agency (ARIS) grants P1-0245, J3-4504, NC-0023, NC-25002 and N3-0394 and by the European Union's Horizon Project Twinning for excellence to strategically advance research in carcinogenesis and cancer (CutCancer; 101079113). The authors also thank the 'PAC Chimie Balard', analytical facilities of Univ Montpellier, CNRS, ENSCM.

Open access publication funding provided by COUPERIN CY26.

Data Availability Statement

The data that support the findings of this study are available from the corresponding author upon reasonable request.

Conflicts of Interest

The authors declare no conflicts of interest.

References

1. C. López-Otín and J. S. Bond, "Proteases: Multifunctional Enzymes in Life and Disease," *Journal of Biological Chemistry* 283 (2008): 30433–30437.

2. E. S. Radisky, "Extracellular Proteolysis in Cancer: Proteases, Substrates, and Mechanisms in Tumor Progression and Metastasis," *Journal of Biological Chemistry* 300 (2024): 107347, https://doi.org/10.1016/j.jbc.2024.107347.

3. A. Aubert, K. Jung, S. Hiroyasu, J. Pardo, and D. J. Granville, "Granzyme Serine Proteases in Inflammation and Rheumatic Diseases," *Nature Reviews Rheumatology* 20 (2024): 361–376, https://doi.org/10.1038/s41584-024-01109-5.

4. T. R. Cox, "The Matrix in Cancer," *Nature Reviews Cancer* 21 (2021): 217–238, https://doi.org/10.1038/s41568-020-00329-7.

5. L. G. N. de Almeida, H. Thode, Y. Eslambolchi, et al., "Matrix Metalloproteinases: From Molecular Mechanisms to Physiology, Pathophysiology, and Pharmacology," *Pharmacological Reviews* 74 (2022): 712–768.

6. K. Kessenbrock, V. Plaks, and Z. Werb, "Matrix Metalloproteinases: Regulators of the Tumor Microenvironment," *Cell* 141 (2010): 52–67, https://doi.org/10.1016/j.cell.2010.03.015.

7. R. E. Vandenbroucke and C. Libert, "Is There New Hope for Therapeutic Matrix Metalloproteinase Inhibition?," *Nature Reviews Drug Discovery* 13 (2014): 904–927, https://doi.org/10.1038/nrd4390.

8. B. Grillet, R. V. S. Pereira, J. Van Damme, A. A. El-Asrar, P. Proost, and G. Opdenakker, "Matrix Metalloproteinases in Arthritis: Towards Precision Medicine," *Nature Reviews Rheumatology* 19 (2023): 363–377, https://doi.org/10.1038/s41584-023-00966-w.

9. E. Hadler-Olsen, B. Fadnes, I. Sylte, L. Uhlin-Hansen, and J.-O. Winberg, "Regulation of Matrix Metalloproteinase Activity in Health and Disease," *Febs Journal* 278 (2011): 28–45, https://doi.org/10.1111/j.1742-4658.2010.07920.x.

10. O. Kollet, A. Das, N. Karamanos, U. Auf dem Keller, and I. Sagi, "Redefining Metalloproteases Specificity Through Network Proteolysis," *Trends in Molecular Medicine* 30 (2024): 147–163, https://doi.org/10.1016/j.molmed.2023.11.001.

11. M. J. Evans and B. F. Cravatt, "Mechanism-Based Profiling of Enzyme Families," *Chemical Reviews* 106 (2006): 3279–3301, https://doi.org/10.1021/cr050288g.

12. K. Kozoriz and J.-S. Lee, "Chemical Proteomics for a Comprehensive Understanding of Functional Activity and the Interactome," *Chemical Society Reviews* 54 (2025): 6186–6207, https://doi.org/10.1039/D5CS00381D.

13. H. Fang, B. Peng, S. Y. Ong, Q. Wu, L. Li, and S. Q. Yao, "Recent Advances in Activity-Based Probes (ABPs) and Affinity-Based Probes (AfBPs) for Profiling of Enzymes," *Chemical Science* 12 (2021): 8288–8310, https://doi.org/10.1039/D1SC01359A.

14. M. Rodriguez-Rios, A. Megia-Fernandez, D. J. Norman, and M. Bradley, "Peptide Probes for Proteases—Innovations and Applications for Monitoring Proteolytic Activity," *Chemical Society Reviews* 51 (2022): 2081–2120, https://doi.org/10.1039/D1CS00798J.

15. H. J. Benns, C. J. Wincott, E. W. Tate, and M. A. Child, "Activity- and Reactivity-Based Proteomics: Recent Technological Advances and Applications in Drug Discovery," *Current Opinion in Chemical Biology* 60 (2021): 20–29, https://doi.org/10.1016/j.cbpa.2020.06.011.

16. F. Meissner, J. Geddes-McAlister, M. Mann, and M. Bantscheff, "The Emerging Role of Mass Spectrometry-Based Proteomics in Drug Discovery," *Nature Reviews Drug Discovery* 21 (2022): 637–654, https://doi.org/10.1038/s41573-022-00409-3.

17. A. Saghatelian, N. Jessani, A. Joseph, M. Humphrey, and B. F. Cravatt, "Activity-Based Probes for the Proteomic Profiling of Metalloproteases," *PNAS* 101 (2004): 10000–10005, https://doi.org/10.1073/pnas.0402784101.

18. S. A. Sieber, S. Niessen, H. S. Hoover, and B. F. Cravatt, "Proteomic Profiling of Metalloprotease Activities With Cocktails of Active-Site Probes," *Nature Chemical Biology* 2 (2006): 274–281, https://doi.org/10.1038/nchembio781.

19. K. C. Ravindra, C. C. Ahrens, Y. Wang, et al., "Chemoproteomics of Matrix Metalloproteases in a Model of Cartilage Degeneration Suggests Functional Biomarkers Associated With Posttraumatic Osteoarthritis," *Journal of Biological Chemistry* 293 (2018): 11459–11469, https://doi.org/10.1074/jbc.M117.818542.

20. C. C. Ahrens, E. L. Chiswick, K. C. Ravindra, et al., "Development and Application of the Metalloprotease Activity Multiplexed Bead-Based Immunoassay (MAMBI)," *Biochemistry* 58 (2019): 3938–3942, https://doi.org/10.1021/acs.biochem.9b00584.

21. A. E. Speers and B. F. Cravatt, "A Tandem Orthogonal Proteolysis Strategy for High-Content Chemical Proteomics," *Journal of the American Chemical Society* 127 (2005): 10018–10019, https://doi.org/10.1021/ja0532842.

22. T. Tamura, M. Kawano, and I. Hamachi, "Targeted Covalent Modification Strategies for Drugging the Undruggable Targets," *Chemical Reviews* 125 (2025): 1191–1253, https://doi.org/10.1021/acs.chemrev.4c00745.

23. K. Shiraiwa, R. Cheng, H. Nonaka, T. Tamura, and I. Hamachi, "Chemical Tools for Endogenous Protein Labeling and Profiling," *Cell Chemical Biology* 27 (2020): 970–985, https://doi.org/10.1016/j.chembiol.2020.06.016.

24. T. Tamura and I. Hamachi, "Chemistry for Covalent Modification of Endogenous/Native Proteins: From Test Tubes to Complex Biological Systems," *Journal of the American Chemical Society* 141 (2019): 2782–2799, https://doi.org/10.1021/jacs.8b11747.

25. M. R. Mortensen, M. B. Skovsgaard, and K. V. Gothelf, "Considerations on Probe Design for Affinity-Guided Protein Conjugation," *Chembiochem* 20 (2019): 2711–2728, https://doi.org/10.1002/cbic.201900157.

26. M. Kaminska, P. Bruyat, C. Malgorn, et al., "Ligand-Directed Modification of Active Matrix Metalloproteases: Activity-Based Probes With no Photolabile Group," *Angewandte Chemie (International ed in English)* 60 (2021): 18272–18279, https://doi.org/10.1002/anie.202106117.

27. C. Malgorn, F. Becher, P. Bruyat, et al., "A New Affinity-Based Probe to Profile MMP Active Forms," *Methods in Molecular Biology* 2747 (2024): 29–39.

28. L. Devel, C. Malgorn, R.-W. Tohon, et al., "Covalent Labeling of Matrix Metalloproteases With Affinity-Based Probes Containing Tuned Reactive N-Acyl-N-Alkyl Sulfonamide Cleavable Linkers," *Chembiochem* 25 (2024): e202400441, https://doi.org/10.1002/cbic.202400441.

29. D. Lascoux, D. Paramelle, G. Subra, et al., "Discrimination and Selective Enhancement of Signals in the MALDI Mass Spectrum of a Protein by Combining a Matrix-Based Label for Lysine Residues With a Neutral Matrix," *Angewandte Chemie (International ed in English)* 46 (2007): 5594–5597, https://doi.org/10.1002/anie.200700811.

30. M. Rossato, G. Miralles, C. M'Kadmi, et al., "Quantitative MALDI-MS Binding Assays: An Alternative to Radiolabeling," *Chemmedchem* 11 (2016): 2582–2587, https://doi.org/10.1002/cmdc.201600447.

31. J. M. Muroski, J. Y. Fu, H. H. Nguyen, R. R. Ogorzalek Loo, and J. A. Loo, "Leveraging Immonium Ions for Targeting Acyl-Lysine Modifications in Proteomic Datasets," *Proteomics* 21 (2021): e2000111, https://doi.org/10.1002/pmic.202000111.

32. D. J. Marchant, C. L. Bellac, T. J. Moraes, et al., "A New Transcriptional Role for Matrix Metalloproteinase-12 in Antiviral Immunity," *Nature Medicine* 20 (2014): 493–502, https://doi.org/10.1038/nm.3508.

33. R. K. Koppisetti, Y. G. Fulcher, A. Jurkevich, et al., "Ambidextrous Binding of Cell and Membrane Bilayers by Soluble Matrix Metalloproteinase-12," *Nature Communications* 5 (2014): 5552, https://doi.org/10.1038/ncomms6552.

34. I. Bertini, V. Calderone, M. Fragai, et al., "Evidence of Reciprocal Reorientation of the Catalytic and Hemopexin-Like Domains of

Full-Length MMP-12," *Journal of the American Chemical Society* 130 (2008): 7011–7021, https://doi.org/10.1021/ja710491y.

35. D. G. Isom, C. A. Castañeda, B. R. Cannon, and B. García-Moreno, "Large Shifts in pKa Values of Lysine Residues Buried Inside a Protein," *PNAS* 108 (2011): 5260–5265, https://doi.org/10.1073/pnas.1010750108.

36. C. K. Engel, B. Pirard, S. Schimanski, et al., "Structural Basis for the Highly Selective Inhibition of MMP-13," *Chemistry & Biology* 12 (2005): 181–189, https://doi.org/10.1016/j.chembiol.2004.11.014.

37. L. Devel, V. Rogakos, A. David, et al., "Development of Selective Inhibitors and Substrate of Matrix Metalloproteinase-12," *Journal of Biological Chemistry* 281 (2006): 11152–11160, https://doi.org/10.1074/jbc.M600222200.

38. A. Adibekian, B. R. Martin, J. W. Chang, et al., "Confirming Target Engagement for Reversible Inhibitors in Vivo by Kinetically Tuned Activity-Based Probes," *Journal of the American Chemical Society* 134 (2012): 10345–10348, https://doi.org/10.1021/ja303400u.

39. S. Deb, J. W. Zhang, and P. E. Gottschall, "Activated Isoforms of MMP-2 Are Induced in U87 Human Glioma Cells in Response to β-amyloid Peptide," *Journal of Neuroscience Research* 55 (1999): 44–53, https://doi.org/10.1002/(SICI)1097-4547(19990101)55:1%3c44::AID-JNR6%3e3.0.CO;2-G.

40. G. Galazka, L. J. Windsor, H. Birkedal-Hansen, and J. A. Engler, "APMA (4-aminophenylmercuric acetate) Activation of Stromelysin-1 Involves Protein Interactions in Addition to Those With Cysteine-75 in the Propeptide," *Biochemistry* 35 (1996): 11221–11227, https://doi.org/10.1021/bi960618e.

41. K. Yamasaki, V. T. G. Chuang, T. Maruyama, and M. Otagiri, "Albumin–Drug Interaction and Its Clinical Implication," *Biochimica Et Biophysica Acta* 1830 (2013): 5435–5443, https://doi.org/10.1016/j.bbagen.2013.05.005.

42. Y. Aida, M. Maeno, N. Suzuki, H. Shiratsuchi, M. Motohashi, and H. Matsumura, "The Effect of IL-1β on the Expression of Matrix Metalloproteinases and Tissue Inhibitors of Matrix Metalloproteinases in Human Chondrocytes," *Life Sciences* 77 (2005): 3210–3221, https://doi.org/10.1016/j.lfs.2005.05.052.

43. C. R. Flannery, C. B. Little, B. Caterson, and C. E. Hughes, "Effects of Culture Conditions and Exposure to Catabolic Stimulators (IL-1 and retinoic acid) on the Expression of Matrix Metalloproteinases (MMPs) and Disintegrin Metalloproteinases (ADAMs) by Articular Cartilage Chondrocytes," *Matrix Biology* 18 (1999): 225–237, https://doi.org/10.1016/S0945-053X(99)00024-4.

44. J. L. Montoya Mira, A. Quentel, R. K. Patel, et al., "Early Detection of Pancreatic Cancer by a High-Throughput Protease-Activated Nanosensor Assay," *Science Translational Medicine* 17 (2025): eadq3110, https://doi.org/10.1126/scitranslmed.adq3110.

45. Q. Zhong, E. K. W. Tan, C. Martin-Alonso, et al., "Inhalable Point-of-Care Urinary Diagnostic Platform," *Science Advances* 10 (2024): eadj9591, https://doi.org/10.1126/sciadv.adj9591.

46. A. P. Amini, J. D. Kirkpatrick, C. S. Wang, et al., "Multiscale Profiling of Protease Activity in Cancer," *Nature Communications* 13 (2022): 5745, https://doi.org/10.1038/s41467-022-32988-5.

47. M. J. Niphakis and B. F. Cravatt, "Ligand Discovery by Activity-Based Protein Profiling," *Cell Chem Biol* 31 (2024): 1636–1651, https://doi.org/10.1016/j.chembiol.2024.08.006.

48. M. Sejalon-Cipolla, P. Bruyat, S. Bregant, et al., "Targeting out of Range Biomolecules: Chemical Labeling Strategies for Qualitative and Quantitative MALDI MS-Based Detection," *TrAC Trends in Analytical Chemistry* 143 (2021): 116399, https://doi.org/10.1016/j.trac.2021.116399.

Supporting Information

Additional supporting information can be found online in the Supporting Information section.

Supporting File: anie71974-sup-0001-SuppMat.pdf.